Integrated Sensing and Communication Waveform Design With Sparse Vector Coding: Low Sidelobe and Ultra Reliability

Ruoyu Zhang, Byonghyo Shim, Weijie Yuan, Marco Di Renzo, Xiaoyu Dang, and Wen Wu

***Abstract*—Integrated sensing and communication (ISAC) can provide efficient usage for both spectrum and hardware resources. A critical challenge, however, is to design the dual-functional waveform for simultaneous radar sensing and communication. In this paper, we propose a sparse vector coding-based ISAC (SVC-ISAC) waveform to simultaneously provide low sidelobe for radar sensing and ultra reliability for communication transmission. The key idea of the proposed waveform is to embed the communication information into the support of one sparse vector and transmit a low-dimensional signal via the spreading codebook. We derive the closed-form expression of ambiguity function, and prove the low sidelobe along both delay and Doppler axes of the proposed SVC-ISAC waveform, regardless of the probability distribution of the transmitted bit stream. Meanwhile, the information decoding at the communication receiver is solved through support identification and sparse demapping. Simulation results demonstrate that the proposed waveform improves the reliability while consistently suppresses the sidelobe level.**

***Index Terms*—Integrated sensing and communication, sparse vector coding, waveform design, ambiguity function, ultra reliability.**

I. Introduction

Integrated sensing and communication (ISAC), supporting both radar sensing and communication functionalities on a single platform and sharing the same frequency band, has been recognized as a promising technique for emerging applications, such as vehicle-to-everything (V2X), multi-function RF systems, unmanned aerial vehicle communication and sensing [1]–[3]. It is expected that such a technique can not only contribute to the efficient usage of spectrum and hardware resources, but also enable the cooperative design of radar and communications [3]–[5].

A critical challenge is to design the dual-functional waveform that can detect radar targets and transmit communication information simultaneously [6]. Early works focused on embedding communication symbols into the radar waveform [7], [8]. In [7], the covert communication information is embedded into the intra or individual pulse of the incident radar waveform. In [8], the phases of the linear frequency modulation waveform for radar are exploited to represent the communications symbols. An alternative strategy of dual-functional waveform design is to tune the widely used communication signals, e.g., orthogonal frequency division multiplexing (OFDM) for radar detection [9]–[11]. The work in [9] investigated the dynamic range and resolution of the OFDM signal, and developed a joint range and Doppler algorithm for the radar target estimation. In [10], the OFDM waveform with a sufficient cyclic prefix has been applied for synthetic aperture radar imaging. To make full use of the spectrum resources, the work in [11] proposed an adaptive OFDM-based joint radar and communications waveform design method with the constraint on the total power. In [12], a communication-embedded OFDM chirp waveform, as well as its ambiguity function (AF), have been investigated for the delay-Doppler radar.

While the goal of these efforts is mainly on the dual-functional waveform design, the sidelobe suppression issue has not been considered [13]–[15]. Due to the randomness of the embedded communication information, it is rather difficult to control the sidelobe level of the integrated sensing and communication waveforms. The work in [16] employed a multiple-phase shift keying direct sequence spread spectrum signal, and developed a recursive least square filter to improve the radar peak sidelobe level. In [17], the weighted summation of communication and radar metrics under per-antenna power budget has been formulated, where the first-order descent algorithm was developed to minimize the range sidelobe. Nevertheless, the communication reliability, which is a crucial performance metric for many future applications such as autonomous driving and V2X [18], fails to be guaranteed in the aforementioned works. To the best of our knowledge, the design of the ISAC waveform providing both low sidelobe and transmission reliability has not been investigated.

In this paper, by exploiting the sparse vector coding (SVC) technique [19], we propose an SVC-based ISAC waveform (SVC-ISAC) to simultaneously achieve low sidelobe and ultra reliability. The key idea of the proposed SVC-ISAC waveform is to embed the communication information into the support of one sparse vector and then transmit the dimension-reduced signal via the spreading codebook. On this basis, we derive the closed-form expression of the AF for the SVC-ISAC waveform, and prove that the proposed SVC-ISAC waveform exhibits the low sidelobe along both delay and Doppler axes, regardless of the probability distribution of the bit stream to be transmitted. In addition, the information decoding at the communication receiver is performed via the support identification based on the sparse recovery and followed by the sparse demapping. Simulation results demonstrate that the proposed SVC-ISAC waveform simultaneously achieves low sidelobe for radar sensing and ultra reliability for communication transmission.

Notations: Vectors and matrices are written in lower-case and upper-case boldface, respectively. $|\Omega|$ denotes the cardinality of the set Ω, while $\|\cdot\|_0$ and $\|\cdot\|_1$ denote the l_0 norm and the l_1 norm, respectively. The operations of transpose, conjugate, and conjugate transpose are denoted by $(\cdot)^T$, $(\cdot)^*$, and $(\cdot)^H$, respectively. $\mathbf{I}_M$ is an identity matrix with dimension $M \times M$, and $\mathrm{j} = \sqrt{-1}$ is an imaginary symbol. $\mathbb{E}[\cdot]$ defines the mathematical expectation, $\mathrm{sinc}(x) = \frac{\sin(\pi x)}{\pi x}$, and $[x]^+$ denotes the operation taking the integer part of a real number x.

II. Proposed SVC-based Integrated Sensing and Communication Waveform

A. Sparse Vector Coding

Let $\mathbf{w}$ be the b-bit information vector to be transmitted. The first step of SVC encoding is to map $\mathbf{w}$ to the L-

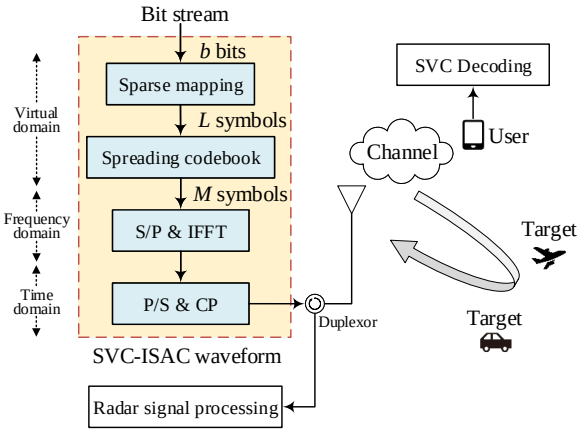

Fig. 1. The block diagram of the proposed SVC-ISAC waveform.

dimensional sparse vector $\mathbf{s}$ with sparsity K (the number of nonzero elements in $\mathbf{s}$ is K). In the second step, each nonzero element in $\mathbf{s}$ is spread into M resources via the spreading sequence $\mathbf{c}_l \in \mathbb{C}^{M\times 1}$. The codebook matrix $\mathbf{C} = [\mathbf{c}_1, \ldots, \mathbf{c}_L]$ is designed such that $\mathbf{Cs}$ contains enough information to recover the sparse vector $\mathbf{s}$ [20]. The corresponding received vector $\mathbf{y}$ is

$$\mathbf{y} = \mathbf{HCs} + \mathbf{v}, \tag{1}$$

where $\mathbf{H}$ and $\mathbf{v}$ are the channel matrix and the additive white Gaussian noise (AWGN), respectively. The decoding of the information vector $\mathbf{w}$ is achieved by identifying nonzero positions in $\mathbf{s}$ and followed by sparse demapping.

B. Proposed SVC-ISAC Waveform

Fig. 1 depicts the block diagram of the proposed SVC-ISAC waveform. Consider the bit stream $\mathcal{W} = \{0, 1\}$, where bit 1 and bit 0 are generated with the probability p_1 and p_0 ($= 1 - p_1$). The bits from $\mathcal{W}$ are divided into N groups, each of which constitutes a b-bit information vector $\mathbf{w}_n \in \mathbb{C}^{b\times 1}$. Let $\Pi_K(\cdot)$ be the SVC encoding operator that performs the sparse mapping, then we have

$$\mathbf{s}_n = \Pi_K(\mathbf{w}_n), \tag{2}$$

where the support set of the L-dimensional sparse vector $\mathbf{s}_n$ is $\Omega_n = \text{supp}(\mathbf{s}_n) = \{l : s_{l,n} \neq 0, 1 \leq l \leq L\}$, $\|\mathbf{s}_n\|_0 = |\Omega| = K$, and the nonzero elements of $\mathbf{s}_n$ satisfy $\boldsymbol{\xi} = \mathbf{s}_{n,\Omega_n}$. By exploiting the predefined spreading codebook $\mathbf{C}_n$ in the virtual domain, we can obtain the dimension-reduced signal $\mathbf{a}_n \in \mathbb{C}^{M\times 1}$ as

$$\mathbf{a}_n = \mathbf{C}_n\mathbf{s}_n = \sum\nolimits_{l\in\Omega_n} \mathbf{c}_{n,l}s_l, \tag{3}$$

where $\mathbf{c}_{n,l}$ is the l-th column of $\mathbf{C}_n$. After the IFFT operation and cyclic prefix (CP) adding, the joint radar-communciation waveform with SVC can be represented by

$$x_{\text{SVC}}(t) = \sum_{n=0}^{N-1}\sum_{m=0}^{M-1} a_{m,n}e^{\text{j}2\pi m\Delta f(t-nT)}u(\frac{t-nT}{T}), \tag{4}$$

where $a_{m,n}$ is m-th element of $\mathbf{a}_n$ in (3), Δf is the subcarrier interval, $T = T_{\text{eff}} + T_{\text{CP}}$ is the duration of one OFDM symbol, where $T_{\text{eff}} = 1/\Delta f$ and T_{CP} are the durations of effective OFDM symbol and CP, respectively, $u(t)$ is the rectangular window function, i.e., $u(t) = 1$, $t \in [0, T]$, and $u(t) = 0$ otherwise. From (2) to (4), we can encode $\lfloor \log_2 \binom{L}{K} \rfloor$ bits of information within one OFDM symbol, and accordingly the spectral efficiency of the SVC-ISAC waveform is $\frac{\lfloor \log_2 \binom{L}{K} \rfloor}{MT\Delta f}$.

The benefits of the proposed SVC-ISAC waveform are threefold: 1) The support of the sparse vector is exploited for the information embedding, which is different from the conventional OFDM signal relying on the amplitudes and phases of constellation points to represent the communication information. 2) The proposed SVC-ISAC waveform inherits the large time and bandwidth product of OFDM signal and is compatible with the OFDM radar receivers [10], so the hardware complexity will not be increased. 3) The proposed waveform artificially constructs the high-dimensional sparse vectors in the virtual domain, realizing the ultra reliability via the transmission diversity.

It is worth pointing out that the spreading codebook $\mathbf{C}_n$ plays an important role in the SVC-ISAC waveform. From the communication perspective, the dimension of the spreading codebook determines the occupied spectrum resources and measurements of recovering the sparse vector $\mathbf{s}_n$, which affects the communication efficiency and reliability, respectively. From the view of radar sensing, the spreading codebook directly generates $a_{m,n}$ on the multiple subcarriers, and accordingly affects the AF performance of the SVC-ISAC waveform.

III. Performance Analysis

In this section, we derive the closed-form expression of AF for the proposed SVC-ISAC waveform and analyze its sidelobe performance in a statistical sense. We also discuss the radar receiver processing for the target detection and the communication receiver for the information decoding.

A. Ambiguity Function Analysis

Ambiguity function is one of the important tools to design and analyze the radar waveforms since it can fully characterize the radar discrimination capability in both range and velocity dimensions. The definition of the ambiguity function for a signal $x(t)$ is given by

$$\chi(\tau, f_{\text{d}}) = \int_{-\infty}^{+\infty} x(t)x^*(t-\tau)e^{\text{j}2\pi f_{\text{d}}t}\text{d}t, \tag{5}$$

where τ and f_{d} are the time delay and the Doppler shift, respectively. By substituting (4) into (5), one can obtain the expression of the proposed SVC-ISAC waveform in (6), where terms γ, τ_1, τ_2, τ_3, and τ_4 are defined by

$$\gamma \triangleq \left[\frac{\tau}{T}\right]^+, -NT < \tau < NT, \tag{7}$$

$$\tau_1 \triangleq \tau + (1 + |\gamma|)T, \tau_2 \triangleq \tau_1 - T, -NT < \tau < 0, \tag{8}$$

$$\tau_4 \triangleq \tau - (1 + |\gamma|)T, \tau_3 \triangleq \tau_4 + T, 0 < \tau < NT. \tag{9}$$

In addition, $\chi^+_{n,n'}(\tau, f_{\text{d}})$ in (10) and $\chi^-_{n,n'}(\tau, f_{\text{d}})$ in (11) denote the cross ambiguity function between the n-th and n'-th symbols for cases $0 < \tau < T$, and $-T < \tau < 0$, respectively. In the following, we provide a lemma describing the statistical behavior of the dimension-reduced signal $\mathbf{a}_n$.

Lemma 1. *Regardless of the bit distribution p_0 or p_1, if the elements of the spreading codebook $\mathbf{C}_n$ and the nonzero elements $\boldsymbol{\xi}$ in the sparse vector $\mathbf{s}_n$ satisfy*

$$p(c_{m,l,n} = 1) = p(c_{m,l,n} = -1) = 1/2, \tag{12}$$

$$\boldsymbol{\xi} = [1, \ldots, K/2, \text{j}, \ldots, \text{j}K/2]^T, \tag{13}$$

$$\chi(\tau,f_{\rm d})=\begin{cases}\sum\limits_{n=1}^{N-1-|\gamma|}e^{{\rm j}2\pi(n-1)f_{\rm d}T}\chi^{+}_{n-1,n+|\gamma|}(\tau_1,f_{\rm d})+\sum\limits_{n=0}^{N-1-|\gamma|}e^{{\rm j}2\pi nf_{\rm d}T}\chi^{-}_{n,n+|\gamma|}(\tau_2,f_{\rm d}), & -NT<\tau<0,\\ \sum\limits_{n'=0}^{N-1-|\gamma|}e^{{\rm j}2\pi(|\gamma|+n')f_{\rm d}T}\chi^{+}_{n'+|\gamma|,n'}(\tau_3,f_{\rm d})+\sum\limits_{n'=1}^{N-1-|\gamma|}e^{{\rm j}2\pi(|\gamma|+n')f_{\rm d}T}\chi^{-}_{n'+|\gamma|,n'-1}(\tau_4,f_{\rm d}), & 0<\tau<NT,\end{cases} \tag{6}$$

$$\chi^{+}_{n,n'}(\tau,f_{\rm d})=(T-\tau)\sum_{m=0}^{M-1}\sum_{m'=0}^{M-1}a_{m,n}a^{*}_{m',n'}e^{{\rm j}2\pi\left((m-m')\Delta f+f_{\rm d}\right)\frac{T+\tau}{2}}e^{{\rm j}2\pi m'\Delta f\tau}{\rm sinc}\Big(\big((m-m')\Delta f+f_{\rm d}\big)(T-\tau)\Big), \tag{10}$$

$$\chi^{-}_{n,n'}(\tau,f_{\rm d})=(T+\tau)\sum_{m=0}^{M-1}\sum_{m'=0}^{M-1}a_{m,n}a^{*}_{m',n'}e^{{\rm j}2\pi\left((m-m')\Delta f+f_{\rm d}\right)\frac{T+\tau}{2}}e^{{\rm j}2\pi m'\Delta f\tau}{\rm sinc}\Big(\big((m-m')\Delta f+f_{\rm d}\big)(T+\tau)\Big), \tag{11}$$

respectively, we have

$$\mathbb{E}\big[a_{m,n}a^{*}_{m',n'}\big]=\begin{cases}\varepsilon, & m=m',n=n',\\ 0, & \text{otherwise},\end{cases} \tag{14}$$

for any positive even number K, where ε is a constant.

Proof. Please see Appendix A. □

Lemma 1 indicates that the transmitted symbols of the proposed SVC-ISAC waveform exhibit the statistically orthogonal property in the frequency domain, and this statistical property is irrelevant to the probability distribution of the input bit stream. With the aid of Lemma 1, we obtain the following theorem.

Theorem 1. *The sidelobe of the ambiguity function for the proposed SVC-ISAC waveform satisfy*

$$\mathbb{E}\big[\chi(\tau,f_{\rm d})\big]=\begin{cases}\psi\big(T-|\tau|\big){\rm sinc}\big(f_{\rm d}(T-|\tau|)\big), & 0<|\tau|<T,\\ 0, & |\tau|\geq T,\end{cases} \tag{15}$$

where $\psi=\varepsilon e^{{\rm j}\pi f_{\rm d}(T+\tau)}\sum_{n=0}^{N-1}e^{{\rm j}2\pi nf_{\rm d}T}\sum_{m=0}^{M-1}e^{{\rm j}2\pi m\Delta f\tau}$.

Proof. The range of the delay τ consists of two parts: $-NT<\tau<0$ and $0<\tau<NT$. We first consider the case $-NT<\tau<0$, which can be further divided into two situations. If the delay satisfies $-NT<\tau\leq -T$, i.e., $-N<\gamma\leq -1$, the expectation value of AF in (6) can be expressed as

$$\begin{aligned}\mathbb{E}\big[\chi(\tau,f_{\rm d})\big]=&\sum_{n=1}^{N-1+\gamma}e^{{\rm j}2\pi(n-1)f_{\rm d}T}\mathbb{E}\big[\chi^{+}_{n-1,n-\gamma}(\tau_1,f_{\rm d})\big]\\ &+\sum_{n=0}^{N-1+\gamma}e^{{\rm j}2\pi nf_{\rm d}T}\mathbb{E}\big[\chi^{-}_{n,n-\gamma}(\tau_2,f_{\rm d})\big]=0,\end{aligned} \tag{16}$$

where the last equality exploits Lemma 1, leading to the results that $\mathbb{E}\big[\chi^{+}_{n-1,n+|\gamma|}(\tau_1,f_{\rm d})\big]=0$ and $\mathbb{E}\big[\chi^{-}_{n,n+|\gamma|}(\tau_2,f_{\rm d})\big]=0$. If $-T<\tau<0$, we have $\gamma=0$. By exploiting Lemma 1, we have $\mathbb{E}\big[\chi^{+}_{n-1,n}(\tau_1,f_{\rm d})\big]=0$ and thus obtain the simplified version of (6) as

$$\begin{aligned}&\mathbb{E}\big[\chi(\tau,f_{\rm d})\big]=\sum_{n=0}^{N-1}e^{{\rm j}2\pi nf_{\rm d}T}\mathbb{E}\big[\chi^{-}_{n,n}(\tau_2,f_{\rm d})\big]\\ &=(T+\tau)\varepsilon\sum_{n=0}^{N-1}e^{{\rm j}2\pi nf_{\rm d}T}\sum_{m=0}^{M-1}e^{{\rm j}\pi f_{\rm d}(T+\tau)}e^{{\rm j}2\pi m\Delta f\tau}{\rm sinc}\big(f_{\rm d}(T+\tau)\big)\\ &=\psi(T+\tau){\rm sinc}\big(f_{\rm d}(T+\tau)\big),-T<\tau<0,\end{aligned} \tag{17}$$

where the second equality follows from (8) in which $\tau_2=\tau+(1+|\gamma|)T-T=\tau$, the last equation holds by defining $\psi=\varepsilon e^{{\rm j}\pi f_{\rm d}(T+\tau)}\sum_{n=0}^{N-1}e^{{\rm j}2\pi nf_{\rm d}T}\sum_{m=0}^{M-1}e^{{\rm j}2\pi m\Delta f\tau}$.

Now we consider the case $0<\tau<NT$ in a similar way. If the delay satisfies $T\leq\tau<NT$, i.e., $1\leq\gamma<N$, we have $\mathbb{E}\big[\chi^{+}_{n'+|\gamma|,n'}(\tau_3,f_{\rm d})\big]=0$ and $\mathbb{E}\big[\chi^{-}_{n'+|\gamma|,n'-1}(\tau_4,f_{\rm d})\big]=0$ with the aid of Lemma 1. Then, the expectation value of AF in (6) simply becomes 0. If $0<\tau<T$, $\gamma=0$, we can obtain $\mathbb{E}\big[\chi^{-}_{n',n'-1}(\tau_4,f_{\rm d})\big]=0$ and the expectation of (6) becomes

$$\begin{aligned}&\mathbb{E}\big[\chi(\tau,f_{\rm d})\big]=\sum_{n'=0}^{N-1}e^{{\rm j}2\pi n'f_{\rm d}T}\mathbb{E}\big[\chi^{+}_{n',n'}(\tau_3,f_{\rm d})\big]\\ &=(T-\tau)\varepsilon\sum_{n'=0}^{N-1}e^{{\rm j}2\pi n'f_{\rm d}T}\sum_{m=0}^{M-1}e^{{\rm j}\pi f_{\rm d}(T+\tau)}e^{{\rm j}2\pi m\Delta f\tau}{\rm sinc}\big(f_{\rm d}(T-\tau)\big)\\ &=\psi(T-\tau){\rm sinc}\big(f_{\rm d}(T-\tau)\big),0<\tau<T,\end{aligned} \tag{18}$$

where the second equality follows from $\tau_3=\tau_4+T=\tau-(1+|\gamma|)T+T=\tau$ in (9) and the last equalit is from the definition of ψ. By combining (17) and (18), we obtain the desired result. □

Theorem 1 reveals that the proposed SVC-ISAC waveform has the low sidelobe along both delay and Doppler axes, no matter what the distribution of 0,1 bits in the input bit stream. Accordingly, the proposed SVC-ISAC waveform exhibits the nearly ideal thumbtack ambiguity function performance in a statistical sense, providing high resolution for target detection when the optimal matched filtering is used.

B. Communication Receiver

In this subsection, we investigate the decoding scheme of the SVC-ISAC waveform in the communication receiver. After sampling (with sampling rate $f_s=M\Delta f$), removing the CP, and performing the discrete fourier transform (DFT), the received signal of the n-th SVC-ISAC symbol in the frequency domain can be represented as

$$\mathbf{y}_n=\mathbf{F}\mathbf{H}\mathbf{F}^{H}\mathbf{a}_n+\mathbf{v}_n, \tag{19}$$

where $\mathbf{y}_n$ is the received signal vector over M subscarriers, $\mathbf{F}\in\mathbb{C}^{M\times M}$ is the DFT matrix, $\mathbf{H}\in\mathbb{C}^{M\times M}$ is the time-domain channel matrix with the first column being $\mathbf{h}=[h_0,h_1,\ldots,h_{P-1},0,\ldots,0]^T$, P is the number of channel taps ($N_{\rm CP}\geq P, N_{\rm CP}=\lceil T_{\rm CP}f_s\rceil$), $\mathbf{v}_n\sim\mathcal{CN}(\mathbf{0},\sigma^2\mathbf{I}_M)$ denotes the AWGN vector of the communication link, the transmit power is denoted by $\rho=\mathbb{E}\big[|a_{m,n}|^2\big]$. In this setup, our goal is to identify the support set Ω behind $\mathbf{a}_n$, rather than directly demodulating the frequency-domain signal $\mathbf{a}_n$. By exploiting (3), we can formulate the SVC decoding as the following sparse signal recovery problem

$$\hat{\mathbf{s}}_n=\arg\min_{\mathbf{s}_n}\|\mathbf{y}_n-\mathbf{G}\mathbf{C}_n\mathbf{s}_n\|_2\quad\text{s.t. }\|\mathbf{s}_n\|_0=K, \tag{20}$$

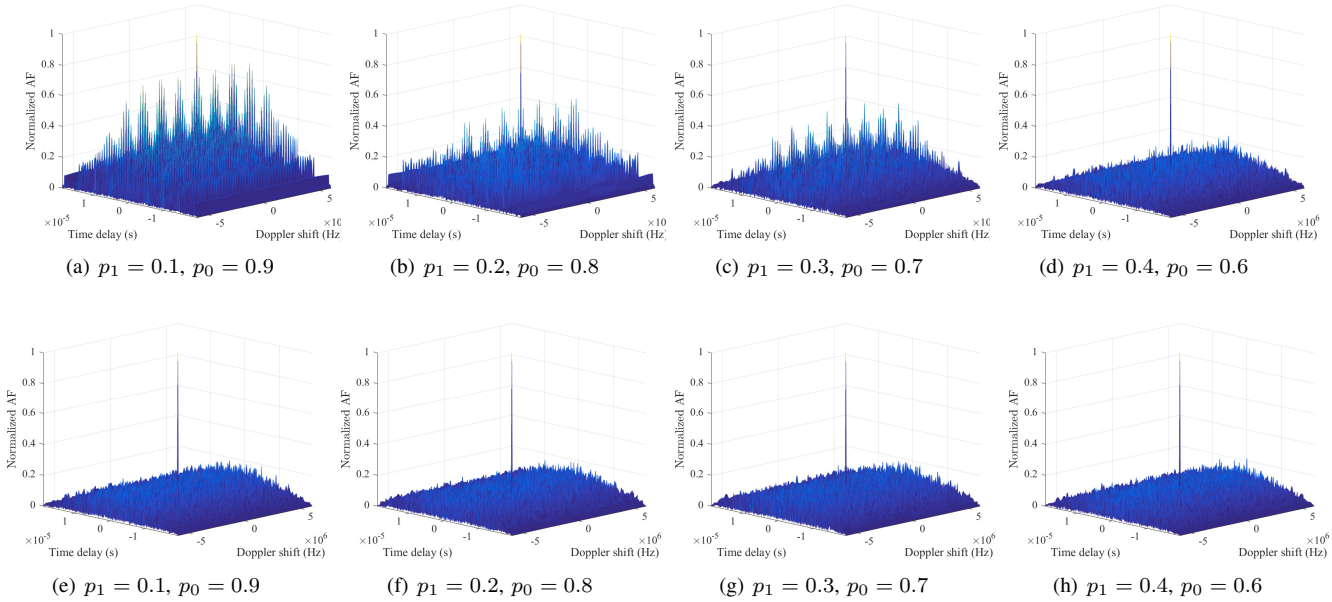

(a) $p_1 = 0.1$, $p_0 = 0.9$ (b) $p_1 = 0.2$, $p_0 = 0.8$ (c) $p_1 = 0.3$, $p_0 = 0.7$ (d) $p_1 = 0.4$, $p_0 = 0.6$

(e) $p_1 = 0.1$, $p_0 = 0.9$ (f) $p_1 = 0.2$, $p_0 = 0.8$ (g) $p_1 = 0.3$, $p_0 = 0.7$ (h) $p_1 = 0.4$, $p_0 = 0.6$

Fig. 2. Comparison of the normalized AF between the OFDM (upper row) and the proposed SVC-ISAC waveform (bottom row) under various bit distribution.

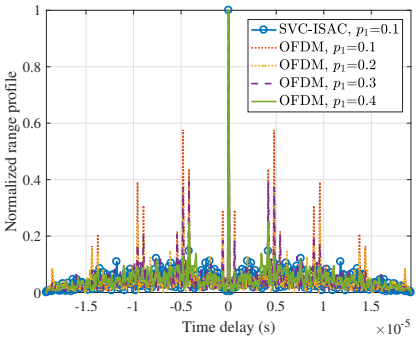

Fig. 3. Comparison of normalized range profiles.

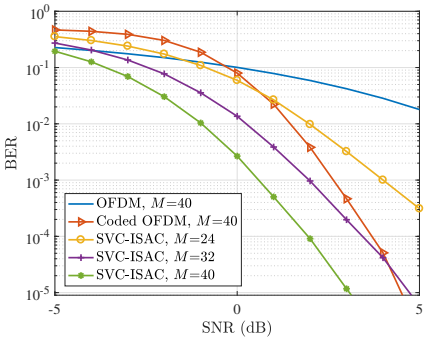

Fig. 4. BER performance as a function of SNR.

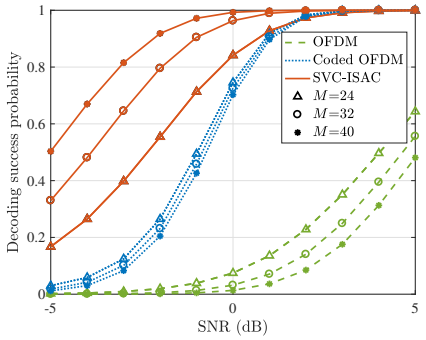

Fig. 5. Decoding success probability versus SNR.

where $\mathbf{G} = \mathbf{FHF}^H$ is the frequency-domain channel matrix. After reconstructing the sparse signal, the support identification can be achieved by extracting the indices of nonzero elements, i.e., $\hat{\Omega} = \text{supp}(\hat{\mathbf{s}}_n)$. Since the sparsity K is also known to the communication receiver in advance, one can find out the solution of $\mathbf{s}_n$ more accurately by using the sparsity-aware recovery techniques [21]. The communication bits information can be decoded via the sparse demapping $\Pi_K^{-1}(\cdot)$ based on the estimated $\hat{\Omega}$. It can be seen from (20) that no channel equalization is needed, which avoids the noise amplification in the zero-forcing method and the high complexity introduced by the minimum mean squared error method.

IV. Simulation Results

In this section, we present the numerical simulations to investigate the radar detection and communication reliability performance of the proposed SVC-ISAC waveform. The simulation parameters are as follows: $\Delta f = 240$ KHz, $M = 40$, $N = 4$, $L = 96$, $K = 2$, $T_{\text{CP}} = 0.15T_{\text{eff}}$. The bit 1 and bit 0 for the original bit stream are generated with the probability p_1 and p_0, respectively. The binary phase shift keying is used for modulation in conventional OFDM signal, while the elements of the spreading codebook $\mathbf{C}_n$ follow from Bernoulli distribution in the SVC-ISAC waveform.

As shown in Fig. 2, we first compare the normalized AF performance of the proposed SVC-ISAC waveform with the conventional OFDM signal when the transmitted communication information follows from different bit distribution p_1, p_0. If $p_1 = 0.1$, the OFDM signal suffers from multiple spurious sidelobe peaks along the axes of both the time delay and the Doppler shift, which may result in the missed or false detection of radar targets. As p_1 and p_0 become closer, the amplitude and quantity of the spurious sidelobes gradually decrease. In contrast, the proposed SVC-ISAC waveform has a nearly ideal thumbtack ambiguity function and exhibits low sidelobe along both delay and Doppler axes for any case of p_1 and p_0. This indicates that the proposed joint radar-communication waveform consistently enjoys the low sidelobe regardless of the bit distribution of the communication information to be transmitted, which validates the theoretical analysis in Theorem 1. We further present the normalized range profile in Fig. 3. It can be observed that the range sidelobe of the conventional OFDM signal is dramatically affected by the bit distribution of the communication information. For the proposed SVC-ISAC waveform, even in the case $p_1 = 0.1$, no

false peak exists in the sidelobe, and the sidelobe magnitude is significantly lower than that of the OFDM signal.

The BER performance of the proposed SVC-ISAC waveform for the communication transmission is depicted in Fig. 4, where the OFDM and coded OFDM (convolutional code with rate 1/2) are also tested for comparison. A frequency-selective fading channel with $P = 6$ taps such that $||\mathbf{h}||_2^2 = 1$ is assumed, and the power delay profile follows from the exponential model. The successive interference cancellation based matching pursuit algorithm in [21] is utilized for support identification in (20). The signal-to-noise ratio (SNR) is defined as $\mathrm{SNR} = \frac{\rho}{\sigma^2}$. We observe that the BER performance of the proposed SVC-ISAC waveform improves gradually with M, and the required SNR for achieving the BER of 10^{-5} is approximately 3 dB when $M = 40$. The proposed joint radar-communication waveform outperforms the coded OFDM signal by around 1.5 dB SNR gain.

Additionally, the decoding success probability as a function of SNR is shown in Fig. 5, where the decoding is declared to be successful if the 0,1 bits in one OFDM symbol are all correctly demodulated. It can be seen that the decoding success probability of the conventional OFDM-based signal gradually decreases due to the increasing information transmission with M. In contrast, a more accurate recovery of sparse vectors is ensured, which is benefited from the decreasing correlation in spreading codewords as M increases. The proposed SVC-ISAC waveform outperforms the coded OFDM signal by a large margin even in the low SNR regime, which demonstrates the ultra reliability of the proposed SVC-ISAC waveform for communication transmission.

V. Conclusion

In this paper, we have proposed the SVC-ISAC waveform by embedding the communication information into the support of one sparse vector and transmitting a low-dimensional signal via the spreading codebook. Thanks to the information embedding with the sparse mapping and random spreading, the proposed dual-functional waveform enhances the performances of both radar and communication. On the one hand, by analyzing the closed-form expression of AF, we have proved that the proposed SVC-ISAC waveform exhibits nearly ideal thumbtack AF and the low sidelobe along both delay and Doppler axes, regardless of the probability distribution of the input bit stream. On the other hand, the information decoding at the communication receiver is based on support identification, providing superior BER performance. Simulation results demonstrate the superiority of the proposed SVC-ISAC waveform in terms of low sidelobe and ultra reliability.

Appendix A
Proof of Lemma 1

Proof. From (3), the m-th element of $\mathbf{a}_n$ is written by $a_{m,n} = \sum_{l\in\Omega} c_{m,l,n} s_{l,n}$. If $K = 2$, i.e., $\boldsymbol{\xi} = [1, \mathrm{j}]^T$, the nonzero entries in $\mathbf{s}_n$ are only either 1 or j, no matter what the values of p_0 or p_1. Under the condition of (12), we can obtain $p(a_{m,n} = 1 + \mathrm{j}) = p(a_{m,n} = 1 - \mathrm{j}) = p(a_{m,n} = -1 + \mathrm{j}) = p(a_{m,n} = -1 - \mathrm{j})$. Denote $a_{m,n} = \varrho e^{\mathrm{j}\vartheta}$, then $\mathbb{E}\big[a_{m,n}a^*_{m',n'}\big] = \mathbb{E}\big[\varrho e^{\mathrm{j}\vartheta}\varrho e^{-\mathrm{j}\vartheta'}\big] = \varrho^2\mathbb{E}\big[e^{\mathrm{j}(\vartheta-\vartheta')}\big]$. Now we consider $\vartheta - \vartheta'$ as a random variable $\bar{\vartheta} \sim \bar{\boldsymbol{\vartheta}}$. If $\vartheta \neq \vartheta'$, the possible values of random variable $\bar{\boldsymbol{\vartheta}}$ are $\{\pm\frac{\pi}{2}, \pm\pi, \pm\frac{3\pi}{2}\}$. Thus, we have $\mathbb{E}\{e^{\mathrm{j}(\vartheta-\vartheta')}\} = \varphi(1) = \mathbb{E}\{e^{\mathrm{j}\bar{\boldsymbol{\vartheta}}}\} = \sum_{\bar{\vartheta}\in\bar{\boldsymbol{\vartheta}}} e^{\mathrm{j}\bar{\vartheta}} p(\bar{\boldsymbol{\vartheta}} = \bar{\vartheta}) = 0$. If $m = m', n = n'$, i.e., $\vartheta = \vartheta'$, we have $\mathbb{E}\{e^{\mathrm{j}(\vartheta-\vartheta')}\} = \varphi(1) = \mathbb{E}\{e^{\mathrm{j}\bar{\boldsymbol{\vartheta}}}\} = p(\bar{\vartheta} = 0)$. By defining the constant $\varepsilon \triangleq \varrho^2 p(\bar{\vartheta} = 0)$, we can obtain (14).

Now we consider $K > 2$ in a similar way. In this case, under the condition of (12) and (13), we have $p(a_{m,n} = d_i) = \frac{1}{K^2}$, where $d_i \in \mathcal{D}$, $|\mathcal{D}| = K^2$, $i = 1, \ldots, K^2$, $\mathcal{D} = \{1 + \mathrm{j}, 1 - \mathrm{j}, \ldots, -\bar{K} - \mathrm{j}\bar{K}\}$, $\bar{K} \triangleq K/2$. Denote $a_{m,n} = \varrho_i e^{\mathrm{j}\vartheta_i}$, $\mathbb{E}\big[a_{m,n}a^*_{m',n'}\big] = \varrho_i\varrho_{i'}\mathbb{E}\big[e^{\mathrm{j}(\vartheta_i-\vartheta_{i'})}\big]$. Consider $\vartheta_i - \vartheta_{i'}$ as a random variable $\bar{\boldsymbol{\vartheta}}_i$. Due to the equal probability of d_i, we have $\mathbb{E}\big[e^{\mathrm{j}(\vartheta_i-\vartheta_{i'})}\big] = \sum_{\bar{\vartheta}_i\in\bar{\boldsymbol{\vartheta}}_i} e^{\mathrm{j}\bar{\vartheta}_i} p(\bar{\boldsymbol{\vartheta}}_i = \bar{\vartheta}_i) = 0$ for $\vartheta_i \neq \vartheta_{i'}$. If $\vartheta_i = \vartheta_{i'}$, then $\mathbb{E}\big[a_{m,n}a^*_{m',n'}\big] = \varrho_i\varrho_{i'}\varrho^2 p(\bar{\vartheta}_i = 0)$. By defining $\varepsilon \triangleq \varrho_i\varrho_{i'} p(\bar{\vartheta}_i = 0)$, the proof is completed. □

References

[1] P. Kumari, J. Choi, N. González-Prelcic, and R. W. Heath, "IEEE 802.11ad-based radar: An approach to joint vehicular communication-radar system," *IEEE Trans. Veh. Technol.*, vol. 67, no. 4, pp. 3012–3027, 2018.

[2] X. Chen, Z. Feng, Z. Wei, F. Gao, and X. Yuan, "Performance of joint sensing-communication cooperative sensing UAV network," *IEEE Trans. Veh. Technol.*, vol. 69, no. 12, pp. 15 545–15 556, 2020.

[3] F. Liu, C. Masouros, A. P. Petropulu, H. Griffiths, and L. Hanzo, "Joint radar and communication design: Applications, state-of-the-art, and the road ahead," *IEEE Trans. Commun.*, vol. 68, no. 6, pp. 3834–3862, 2020.

[4] L. Zheng, M. Lops, Y. C. Eldar, and X. Wang, "Radar and communication coexistence: An overview: A review of recent methods," *IEEE Signal Process. Mag.*, vol. 36, no. 5, pp. 85–99, 2019.

[5] D. Ma, N. Shlezinger, T. Huang, Y. Liu, and Y. C. Eldar, "Joint radar-communication strategies for autonomous vehicles: Combining two key automotive technologies," *IEEE Signal Process. Mag.*, vol. 37, no. 4, pp. 85–97, 2020.

[6] A. Hassanien, M. G. Amin, Y. D. Zhang, and F. Ahmad, "Signaling strategies for dual-function radar communications: An overview," *IEEE Aerosp. Electron. Syst. Mag.*, vol. 31, no. 10, pp. 36–45, 2016.

[7] S. D. Blunt, J. G. Metcalf, C. R. Biggs, and E. Perrins, "Performance characteristics and metrics for intra-pulse radar-embedded communication," *IEEE J. Sel. Areas Commun.*, vol. 29, no. 10, pp. 2057–2066, 2011.

[8] M. J. Nowak, Z. Zhang, L. LoMonte, M. Wicks, and Z. Wu, "Mixed-modulated linear frequency modulated radar-communications," *IET Radar Sonar Navig.*, vol. 11, no. 2, pp. 313–320, 2016.

[9] C. Sturm and W. Wiesbeck, "Waveform design and signal processing aspects for fusion of wireless communications and radar sensing," *Proc. IEEE*, vol. 99, no. 7, pp. 1236–1259, 2011.

[10] T. Zhang and X. Xia, "OFDM synthetic aperture radar imaging with sufficient cyclic prefix," *IEEE Trans. Geosci. Remote Sens.*, vol. 53, no. 1, pp. 394–404, 2015.

[11] Y. Liu, G. Liao, J. Xu, Z. Yang, and Y. Zhang, "Adaptive OFDM integrated radar and communications waveform design based on information theory," *IEEE Commun. Lett.*, vol. 21, no. 10, pp. 2174–2177, 2017.

[12] M. Li, W.-Q. Wang, and Z. Zheng, "Communication-embedded OFDM chirp waveform for delay-Doppler radar," *IET Radar Sonar Navig.*, vol. 12, no. 3, pp. 353–360, 2017.

[13] M. A. Richards, *Fundamentals of Radar Signal Processing, Second Edition*. McGraw-Hill Education, 2005.

[14] G. Hua and S. S. Abeysekera, "Receiver design for range and Doppler sidelobe suppression using MIMO and phased-array radar," *IEEE Trans. Signal Process.*, vol. 61, no. 6, pp. 1315–1326, 2013.

[15] J.-C. Chen, C.-K. Wen, and K.-K. Wong, "An efficient sensor-node selection algorithm for sidelobe control in collaborative beamforming," *IEEE Trans. Veh. Technol.*, vol. 65, no. 8, pp. 5984–5994, 2016.

[16] L. Tang, K. Zhang, H. Dai, P. Zhu, and Y.-C. Liang, "Analysis and optimization of ambiguity function in radar-communication integrated systems using MPSK-DSSS," *IEEE Wireless Commun. Lett.*, vol. 8, no. 6, pp. 1546–1549, 2019.

[17] F. Liu, C. Masouros, T. Ratnarajah, and A. Petropulu, "On range sidelobe reduction for dual-functional radar-communication waveforms," *IEEE Wireless Commun. Lett.*, vol. 9, no. 9, pp. 1572–1576, 2020.

[18] X. Ge, "Ultra-Reliable Low-Latency Communications in Autonomous Vehicular Networks," *IEEE Trans. Veh. Technol.*, vol. 68, no. 5, pp. 5005–5016, May 2019.

[19] H. Ji, S. Park, and B. Shim, "Sparse vector coding for ultra reliable and low latency communications," *IEEE Trans. Wireless Commun.*, vol. 17, no. 10, pp. 6693–6706, Oct. 2018.

[20] W. Kim, S. K. Bandari, and B. Shim, "Enhanced sparse vector coding for ultra-reliable and low latency communications," *IEEE Trans. Veh. Technol.*, vol. 69, no. 5, pp. 5698–5702, Nov. 2020.

[21] R. Zhang, B. Shim, Y. Lou, S. Jia, and W. Wu, "Sparse vector coding aided ultra-reliable and low-latency communications in multi-user massive MIMO systems," *IEEE Trans. Veh. Technol.*, vol. 70, no. 1, pp. 1019–1024, 2021.